American Mineralogist, Volume 105, pages 1436–1440, 2020

Letter

Inherited Eocene magmatic tourmaline captured by the Miocene Himalayan leucogranites

Jinsheng Han[1], Pete Hollings[2], Fred Jourdan[3], Yunchuan Zeng[4], and Huayong Chen[1,*]

[1]Key Laboratory of Mineralogy and Metallogeny, Guangzhou Institute of Geochemistry, Chinese Academy of Sciences, Guangzhou 510640, China

[2]Department of Geology, Lakehead University, 955 Oliver Road, Thunder Bay, Ontario P7B 5E1, Canada

[3]Western Australian Argon Isotope Facility, Department of Applied Geology and JdL-CMS, Curtin University, GPO Box U1987, Perth, Western Australia 6845, Australia

[4]State Key Laboratory of Geological Processes and Mineral Resources, School of Earth Science and Resources, China University of Geosciences, Beijing 100083, China

Abstract

The Miocene Cuonadong leucogranites in the easternmost section of the Tethyan Himalaya, Southern Tibet, are characterized by two types of tourmaline. Tourmaline occurs as needle-like crystals in the two-mica ± tourmaline granites (Tur G) and large patches in the pegmatites (Tur P). Both the granite and the pegmatites yield Miocene ages (ca. 20 Ma) based on monazite U(-Th)-Pb dating, whereas $^{40}Ar/^{39}Ar$ geochronology of the coarse-grained tourmalines (Tur P) crosscut by pegmatite veins yielded an Eocene mini-plateau age of 43 ± 6 Ma. Major element concentrations of tourmaline indicate that both Tur P and Tur G belong to the schorl group with a magmatic origin, but trace elements such as V indicate that they are not cogenetic. Boron isotopes suggest that Tur P (average –9.76‰) was derived from typical crustal sources, whereas Tur G (average –7.65‰) contains relatively more mafic input. The capture of Eocene tourmaline by the Miocene leucogranites at Cuonadong suggests that the crustally derived Eocene magmatism may have occurred in the southern Tethyan Himalaya. Identification of the inherited magmatic tourmaline (Tur P), although not common, challenges the current application of tourmaline chemistry to the investigation of magmatic-hydrothermal systems.

Keywords: Inherited tourmaline, Himalayan leucogranite, $^{40}Ar/^{39}Ar$ and U(-Th)-Pb geochronology, B isotope

Introduction

The Himalayan continent-continent collisional belt resulted from the convergence and collision of India and Asia along the Indus-Tsangpo Suture zone that began in the Cenozoic (Yin and Harrison 2000). Crustal anatexis related to this large-scale continental collision resulted in the formation of a series of leucogranites (Yin 2006), which generally consist of cogenetic two-mica-, tourmaline-, and garnet-bearing rocks with widespread dikes and stocks of pegmatite (Wu et al. 2020). Two sub-parallel E-trending leucogranite belts, the Higher Himalayan and Tethyan Himalayan (Supplemental[1] Figs. S1a and S1b), have been recognized, with the former exposed along the South Tibetan Detachment System (STDS) in the Higher Himalayan Sequence (HHS) and the latter mainly occurring in the core of the North Himalayan Gneiss Domes (NHGDS) (Supplemental[1] Fig. S1b; Wu et al. 2020). The majority of the leucogranites have yielded Miocene ages (26–7 Ma), with a small number of samples with Eocene ages (46–30 Ma) being found in the eastern most region of the Tethyan Himalayan (Wu et al. 2020). The Miocene and Eocene leucogranites were proposed to have formed from distinct episodes of crustal anatexis with clearly separated distribution in Southern Tibet (Supplemental[1] Fig. S1; Patiño Douce and Harris 1998; Hou et al. 2012). Tourmaline, which is very common in the Himalayan leucogranites and typically the dominant reservoir of B in the rocks, is stable in various *P-T-X* conditions and could record the physical and chemical conditions under which it formed (Marschall and Jiang 2011; Slack and Trumbull 2011). Due to its robustness, tourmaline chemistry has recently been used to investigate the genesis of Himalayan leucogranites (Yang et al. 2015; Hu et al. 2018). However, these studies relied on the assumption that the tourmalines formed cogenetically with their magmatic host rocks as is widely interpreted in most of the global tourmaline occurrences (van Hinsberg et al. 2011). Following the approach illustrated by Thern et al. (2020), we applied the $^{40}Ar/^{39}Ar$ dating method to coarse-grained tourmalines from the Miocene Cuonadong leucogranite, which yielded Eocene ages. The identification of inherited tourmalines not only contributes new insights into the Himalayan collisional orogeny but also provides constraints on application of tourmaline chemistry to petrological studies.

Cuonadong tourmaline petrography

The Cuonadong leucogranite is located in the easternmost section of the Tethyan Himalaya (Supplemental[1] Fig. S1a) and consists mainly of two-mica ± tourmaline granite and granitic pegmatite. The pegmatites commonly occur as veins or pockets in the leucogranites, without clear boundaries between them (Supplemental[1] Fig. S2). The wall rocks consist mainly of sandstone, mudstone, slate, and schist intercalated with carbonates (Li et al. 2017; Zhou et al. 2019). Two types of tourmalines have been identified in the Cuonadong leucogranites, large tourmaline crystals in the pegmatites (Tur P; Figs. 1a–d) and needle-like tourmaline crystals in the two-mica ± tourmaline granite (Tur G; Fig. 1e). The Tur P are

* E-mail: huayongchen@gig.ac.cn

0003-004X/20/0009–1436$05.00/DOI: https://doi.org/10.2138/am-2020-7608

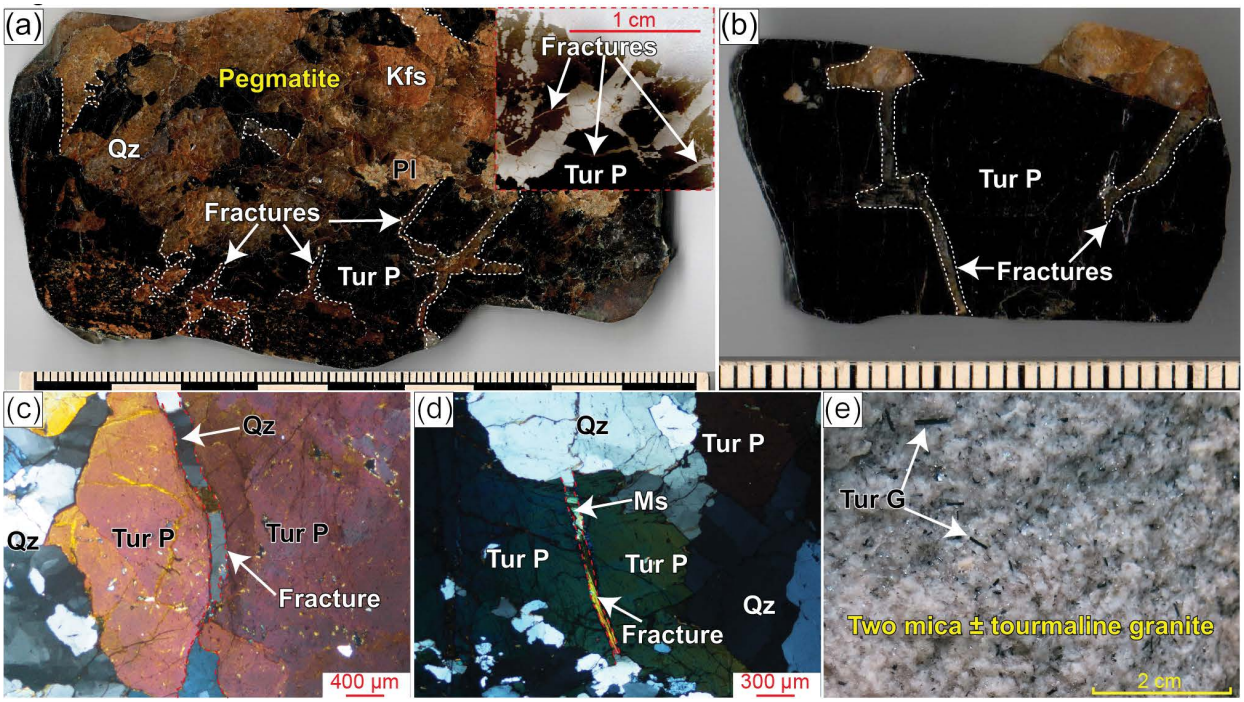

Figure 1. (**a**) Hand specimen of the Cuonadong pegmatites, showing abundant fractures in the tourmaline grains. A part of a thin section was scanned as insert, showing the common occurrences of fractures in Tur P. (**b**) Another sample of the Cuonadong pegmatites showing fractured tourmaline. (**c**) Photomicrograph showing Tur P crosscut by a quartz vein in pegmatite. (**d**) Photomicrograph showing Tur P crosscut by a quartz-muscovite vein in pegmatite. (**e**) The crystal habit of tourmaline (Tur G) in the two-mica ± tourmaline granite. (Color online.)

pervasively distributed in the pegmatites and are cut by abundant quartz/pegmatite/quartz-muscovite veins along fractures (Figs. 1a–d; Supplemental[1] Fig. S3a). Abundant micro-fractures and some zircon inclusions were observed in the Tur P in backscattered electron (BSE) images (Supplemental[1] Fig. S3b). The Tur G occur as disseminated needle-like crystals coexisting with muscovite, quartz, and feldspar in the granites and that show clear core-rim zoning in thin section but not in BSE images (Fig. 1e, Supplemental[1] Figs. S2c and S2d). Both Tur P and Tur G are commonly homogeneous in BSE images.

Methods

Tourmaline $^{40}Ar/^{39}Ar$ analyses were performed on one pegmatite sample using an ARGUS VI at the Western Australian Argon Isotope Facility, Curtin University. Monazite LA ICP-MS U(-Th)-Pb geochronology of both granite and pegmatite was performed utilizing a system consisting of ASI RESOlution S-155 193 nm ArF Excimer laser coupled to Thermo-Scientific iCAP Qc quadrupole ICP-MS at the State Key Laboratory for Mineral Deposits Research, Nanjing University, China. The detailed analytical procedures and conditions of all the above and other methods are listed in Supplemental[1] Appendix A.

Results

The Tur P in the pegmatites yielded a $^{40}Ar/^{39}Ar$ mini-plateau age of 43 ± 6 Ma (MSWD = 0.8; P = 0.57; Supplemental[1] Table S1; Fig. 2a), which includes 66.3% of the total amount of ^{39}Ar that was released. Commonly for low potassium minerals containing excess argon, a saddle-shaped ^{39}Ar release spectrum during stepped heating will be displayed (Kelley 2002), which is not shown in our Tur P data indicating the absence of excess ^{40}Ar in the lattice during crystallization (Qiu et al. 2007), suggesting that the calculated Ar plateau age represents the true age of tourmaline, rather than the result of excess argon. The high apparent step ages (older than 70 Ma) displayed within the first few percent of gas released are likely attributed to excess ^{40}Ar in fluid inclusions or the margins of the crystals. We calculated a mini-inverse isochron age of 58 ± 15 Ma (MSWD = 0.8; P = 0.63), associated with a trap $^{40}Ar/^{36}Ar$ ratio of 251 ± 52. This ratio, although imprecise, does overlap with atmospheric compositions (~298.6; Lee et al. 2006), which would indicate the mini-plateau age (which assumes a $^{40}Ar/^{36}Ar$ ratio of 298.6) is correct. Note that a sub-atmospheric ratio and the absence of saddle-shaped ^{39}Ar release spectrum suggest that no excess ^{40}Ar is present in this part of the age spectrum. In addition, some monazite grains in the granite yielded similar ages to the mini-plateau age (Fig. 2b). In general, the mini-plateau and mini-inverse isochron ages of 43 ± 6 and 58 ± 15 Ma (Fig. 2a), respectively, overlap with each other and are both clearly older than the U-Th-Pb age of ca. 20 Ma for the monazite (Figs. 2b and 2c).

Monazite often has excess ^{206}Pb, resulting in high $^{206}Pb/^{238}U$ age and reverse discordance on U-Pb diagrams (Schärer 1984). Thus, the $^{207}Pb/^{235}U$ may provide the best estimate of the age. However, the Himalaya leucogranites are too young to yield reliable $^{207}Pb/^{235}U$ (Wu et al. 2015). As a result, the Th-Pb ages are often used for monazite geochronology of the Himalaya leucogranites (Harrison et al. 1995). Monazite grains from the two-mica ± tourmaline granite sample yielded a $^{208}Pb/^{232}Th$ age of 20.3 ± 0.2 Ma, with two grains having older ages of 45.2 ± 1.6 and 43.9 ± 1.4 Ma (Supplemental[1] Table S2; Fig. 2b). The older ages are consistent with the plateau $^{40}Ar/^{39}Ar$ age of the Tur P and represent inherited monazite crystals. The pegmatite sample yielded a monazite $^{208}Pb/^{232}Th$ age of 20.5 ± 0.1 Ma (Supplemental[1] Table S2; Fig. 2c), nearly identical to

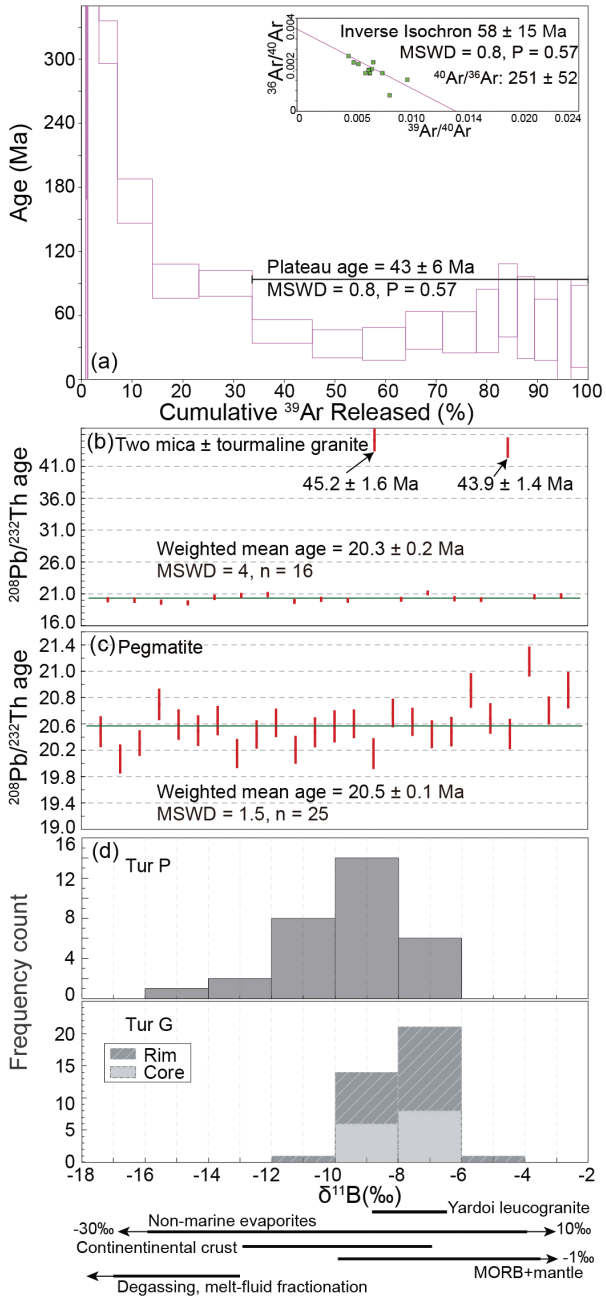

Figure 2. (**a**) Plateau $^{40}Ar/^{39}Ar$ dating results, and $^{36}Ar/^{40}Ar$ vs. $^{39}Ar/^{40}Ar$ normal and inverse isochron plots of the Tur P. (**b** and **c**) Monazite geochronological results of the Cuonadong leucogranites. (**d**) Boron isotope compositions of the Tur P and Tur G and comparison with various boron reservoirs in nature (after Marschall and Jiang 2011; Hu et al. 2018). (Color online.)

the two-mica granite ages and distinct from the plateau $^{40}Ar/^{39}Ar$ age of Tur P.

Major and trace element compositions of the tourmaline are provided in Supplemental[1] Table S3. Both Tur P and Tur G are dominantly schorl end-member tourmalines, with Fe/(Fe+Mg) ratios of 0.67–0.85 for Tur P, 0.75–0.87 for the Tur G cores and 0.74–0.87 the Tur G rims. Tourmaline grains have wide ranges of Ti (0.04–0.15 apfu for the Tur P, 0.01–0.09 apfu for the Tur G core, 0.02–0.11 apfu for the Tur G rim) and Al concentrations (6.23–6.55 apfu for the Tur P, 6.04–6.50 apfu for the Tur G core and 6.00–6.70 apfu for the Tur G rim). On the Al-Fe-Mg diagram, both the Tur P and the Tur G plot in the field of Li-poor granitoids and associated pegmatites and aplites, suggesting a magmatic origin (Supplemental[1] Fig. S4). The trace element compositions in tourmaline are commonly low, from tens of parts per million for the large ion lithophile elements (LILE) to ppb for the high field strength elements (HFSE). The concentrations of Cr, Co, Ni, Sr, V, and Sc in Tur P are commonly higher than those of the Tur G. The Tur P have a wider range and lower average $\delta^{11}B$ values than the Tur G, with the former ranging from –14.14‰ to –7.06‰ (average –9.76‰) and the latter from –8.82‰ to –6.79‰ (average –7.69‰, Tur G core) and –10.25‰ to –5.83‰ (average –7.61‰, Tur G rim; Fig. 2d), respectively. The $\delta^{11}B$ values for Tur P and Tur G are well within the range reported for other granites in the world (Supplemental[1] Table S4; ca. –15% and ca. –5%, Marschall and Jiang 2011).

Discussion and implications

Tourmaline is common in highly evolved granites and pegmatites and has been widely used to investigate their petrogenesis (e.g., Yang et al. 2015) and to decipher the process of fluid flow during the magmatic-hydrothermal transition (Launay et al. 2018). All of these studies depend on the assumption that the formation of the tourmaline was coeval with, and has a genetic connection to, the host rocks. Our work at Cuonadong shows that some tourmalines in the granite/pegmatite may be inherited and thus unrelated to the host granite. Two lines of evidence support the inherited origin of Tur P. (1) Monazite grains in the pegmatites and two-mica ± tourmaline granites yielded ages of ca. 20 Ma (Fig. 2b), whereas the Tur P $^{40}Ar/^{39}Ar$ dating yielded an Eocene age of ca. 40 Ma, coinciding with the presence of two Eocene monazite grains in the granite (Figs. 2a and 2b), and significantly older than the crystallization age of the host pegmatites. (2) The common occurrence of fractures in these tourmalines and the presence of the pegmatite mineral assemblages in the fractures suggests that they predate the pegmatites (Figs. 1a–d).

Several lines of evidence suggest that the two-mica granite and pegmatite evolved in a cogenetic system, with the pegmatite magmas representing the late evolved phase. (1) They yield comparable ages. (2) Both the granite and pegmatite have similar mineral assemblages consisting of plagioclase, k-feldspar, muscovite ± tourmaline. (3) The occurrences of the pegmatites as veins or pockets in the granites, without clear boundaries between them (Supplemental[1] Fig. S2). (4) Xie et al. (2020) studied zircon grains in the granite and pegmatite at Cuonadong and proposed magmatic evolution from the granites to pegmatites based on the Zr/Hf ratios of zircon.

However, Tur P should be xenocrysts in the host granitoids. In a cogenetic system, tourmaline crystallized in early-stage granite should have higher V contents compared to those formed in a late pegmatite because V is preferentially fractionated into early-crystallized ilmenite, biotite, and tourmaline during magma crystallization (van Hinsberg 2011). Therefore, if Tur P is a primary phase in the host pegmatite, it should have lower V contents than

Tur G, which represents the early crystallization stage (two-mica granite). However, the obviously higher V concentrations in Tur P suggest that it was not a product of the same Miocene magmatism as the host pegmatite (Supplemental[1] Table S3).

What was the source of the Eocene Tur P and how was it incorporated in the Miocene leucogranite? Based on $^{40}Ar/^{39}Ar$ geochronology, the Tur P formed at ca. 40 Ma. These ages are coeval with the emplacement ages of the Yardoi granitoids (Zeng et al. 2011; Hou et al. 2012), which is ca. 100 km north of Cuonadong and one of the few occurrences of Eocene intrusions in the northern Tethyan Himalaya (Supplemental[1] Fig. S1). The Yardoi granitoids were interpreted to have formed from the partial melting of the lower crust of the India plate during Eocene crustal thickening and the subsequent Neo-Tethyan slab break-off in the early stage of the India-Asian collision (Fig. 3a; Zeng et al. 2011; Hou et al. 2012). Tourmalines are not common in the Yardoi granitoids, but recent boron isotope analyses showed that the $\delta^{11}B$ values of the Yardoi granitoids range from –8.9‰ to –6.6‰ (Fig. 2c; Hu et al. 2018), partially overlapping with those of Tur P having ranges of –14.14‰ to –7.06‰ (average –9.76‰). However, ^{11}B values for Tur P are relatively lighter, approximating the average boron isotopes of continental crust (–10 ± 3‰, Marschall and Jiang 2011), whereas the Yardoi and the Miocene tourmalines at Cuonadong (Tur G) have higher $\delta^{11}B$ values. The differences may suggest more involvement of lower crust (mafic magma) during crustal anatexis for the latter (Fig. 2d), supported by regional tectonic evolution models for the Eocene Yardoi granitoids and Miocene Cuonadong leucogranite (Hou et al. 2012; Wu et al. 2020). We propose that partial melting of upper crustal materials may have occurred in the Cuonadong area during Eocene crustal thickening, when shear heating elevated the surface heat flow (Hartz and Podladchikov 2008), causing the temperature to reach the solidus, generating the felsic magmatism and forming Tur P (Figs. 3a). During later geologic events, the Tur P was preserved due to their robustness (Marschall and Jiang 2011; Slack and Trumbull 2011). The widespread Miocene leucogranite magmatism (including the early-stage two-mica granite and late evolved pegmatite phase), formed either by decompressional melting of the crust (Wu et al. 2020) or extensive long-living shear heating (Whittington et al. 2009; Hou et al. 2012) linked to Indian plate rollback and break off (DeCelles et al. 2011). The magma ascended to the upper crust (Fig. 3a) where the late pegmatite phase in the upper part of the two-mica granite incorporated the early-stage Eocene granitoids and Tur P at shallow levels in the crust (Figs. 3b and 3c). Although no Eocene tourmaline has been found in the two-mica granite, the presence of Eocene-age monazite xenocrysts (Fig. 2b) are consistent with the assimilation of Eocene granites by the Miocene granite at Cuonadong.

Our studies document the spatial coexistence of Miocene and

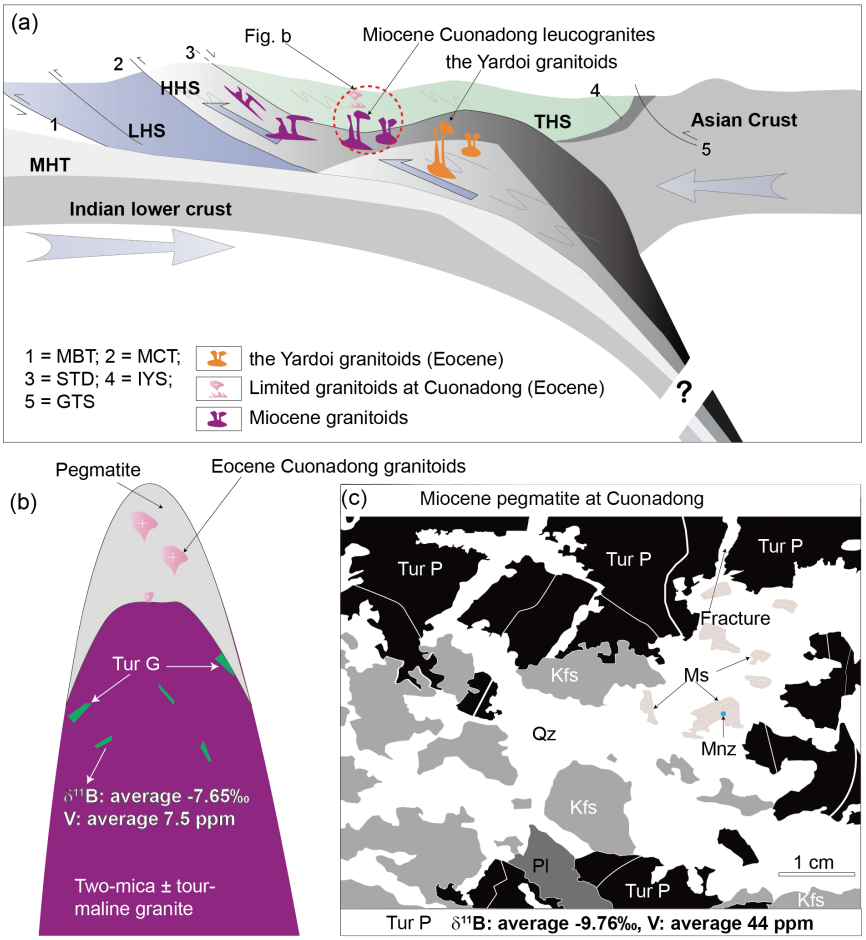

FIGURE 3. (**a**) Schematic regional section showing the Eocene Yardoi granitoids and granitoids at Cuonadong (100 km south to Yardoi) during crustal thickening. The large-scale Miocene Himalayan leucogranites due to intense activity of the STD and HHS extrusion emplaced at Cuonadong area. STD = South Tibetan Detachment; MCT = Main Central Thrust; MBT = Main Boundary Thrust; HHS = High Himalayan Sequence; THS = Tethyan Himalayan Sequence; IYS = Indus-Yarlung suture; GTS = Gangdese thrust system. (**b**) A simplified cartoon for emplacement of the Miocene Cuonadong leucogranites, represented by the two-mica granite and the late cogenetic pegmatite phase, and xenoliths of the Eocene granitic units containing Tur P. (**c**) Schematic diagram showing the capture of the Eocene Tur P by the Miocene pegmatites at Cuonadong. Pl = plagioclase; Qz = quartz; Kfs = K-feldspar; Mnz = monazite; Ms = muscovite. (Color online.)

Eocene magmatism in the Tethyan Himalaya and suggest petrogenesis through upper crust anatexis during shear heating for the Eocene magmas in Southern Tibet. The presence of inherited tourmaline means that the K/Ar clock in the tourmaline was not reset by thermal diffusion during the emplacement of the granitic pegmatite, perhaps due to the high closure temperature and low diffusion rates for major and trace elements within the tourmaline structure (Dutrow and Henry 2011). Thus, caution must be used when applying tourmaline geochemistry to the investigation of the petrogenesis of the host magmatic rocks.

Acknowledgments and Funding

We appreciate comments by Calvin Barnes, Nadia Mohammadi, and an anonymous reviewer on this paper. This study was funded by the National Natural Science Foundation of China (41725009), and the Fundamental and Applied Fundamental Research Major Program of Guangdong Province (2019B030302013). This is contribution no. IS-2877 from GIGCAS.

References cited

DeCelles, P.G., Kapp, P., Quade, J., and Gehrels, G.E. (2011) Oligocene–Miocene Kailas basin, southwestern Tibet: Record of postcollisional upper-plate extension in the Indus-Yarlung suture zone. Geological Society of America Bulletin, 123, 1337–1362.

Dutrow, B.L., and Henry, D.J. (2011) Tourmaline: A Geologic DVD. Elements, 7, 301–306.

Harrison, T.M., Mckeegan, K.D., and LeFort, P. (1995) Detection of inherited monazite in the Manaslu leucoganite by $^{208}Pb/^{232}Th$ ion microprobe dating. Chemical Geology, 133, 271–282.

Hartz, E.H., and Podladchikov, Y.Y. (2008) Toasting the jelly sandwich: The effect of shear heating on lithospheric geotherms and strength. Geology, 36, 331–334.

Hou, Z.Q., Zheng, Y.C., Zeng, L.S., Gao, L.E., Huang, K.X., Li, W., Li, Q.Y., Fu, Q., Liang, W., and Sun, Q.Z. (2012) Eocene–Oligocene granitoids in southern Tibet: Constraints on crustal anatexis and tectonic evolution of the Himalayan orogen. Earth and Planetary Science Letters, 349-350, 38–52.

Hu, G.Y., Zeng, L.S., Gao, L.E., Liu, Q.P., Chen, H., and Guo, Y.S. (2018) Diverse magma sources for the Himalayan leucogranites: Evidence from B-Sr-Nd isotopes. Lithos, 314-315, 88–99.

Kelley, S. (2002) Excess argon in K–Ar and Ar–Ar geochronology. Chemical Geology, 188, 1–22.

Launay, G., Sizaret, S., Guillou-Frottier, L., Gloaguen, E., and Pinto, F. (2018) Deciphering fluid flow at the magmatic-hydrothermal transition: A case study from the world-class Panasqueira W–Sn–(Cu) ore deposit (Portugal). Earth and Planetary Science Letters, 499, 1–12.

Lee, J.Y., Marti, K., Severinghaus, J.P., Kawamura, K., Yoo, H.S., Lee, J.B., and Kim, J.S. (2006) A redetermination of the isotopic abundances of atmospheric Ar. Geochimica et Cosmochimica Acta, 70, 4507–4512.

Li, G.M., Zhang, L.K., Jiao, Y.J., Xia, X.B., Dong, S.L., Fu, J.G., Liang, W., Zhang, Z., Wu, J.Y., Dong, L., and Huang, Y. (2017) First discovery and implications of Cuonadong superlarge Be-W-Sn polymetallic deposit in Himalayan metallogenic belt, southern Tibet. Mineral Deposits, 36, 1003–1008 (in Chinese with English abstract).

Marschall, H.R., and Jiang, S.Y. (2011) Tourmaline Isotopes: No Element Left Behind. Elements, 7, 313–319.

Patiño Douce, A.E., and Harris, N. (1998) Experimental constraints on Himalayan anatexis. Journal of Petrology, 39, 689–710.

Qiu, H.N., Pu, Z.P., and Dai, T.M. (2007) Occurrences of excess ^{40}Ar in hydrothermal tourmaline: Interpretations from ^{40}Ar-^{39}Ar dating results by stepwise heating. Acta Geologica Sinica, 81, 51–516.

Schärer, U. (1984) The effect of initial ^{230}Th disequilibrium on young U/Pb ages: the Makalu case, Himalaya. Earth and Planetary Science Letters, 67, 191–204.

Slack, J.F., and Trumbull, R.B. (2011) Tourmaline as a recorder of ore-forming processes. Elements, 7, 321–326.

Thern, E.R., Blereau, E., Jourdan, F., and Nelson, D.R. (2020) Tourmaline $^{40}Ar/^{39}Ar$ geochronology and thermochronology: Example from the youngest Hadean-zircon-bearing siliciclastic metasedimentary rocks from the Yilgarn Craton. Geochimica et Cosmochimica Acta, 277, 285–299.

van Hinsberg, V.J. (2011) Preliminary experimental data on trace element partitioning between tourmaline and silicate melt. Canadian Mineralogist, 49, 153–163.

van Hinsberg, V.J., Henry, D.J., and Dutrow, B.L. (2011) Tourmaline as a petrologic forensic mineral: A unique recorder of its geologic past. Elements, 7, 327–332.

Whittington, A.G., Hofmeister, A.M., and Nabelek, P.I. (2009) Temperature-independent thermal diffusivity of the Earth's crust and implication for magmatism. Nature, 458, 319–321.

Wu, F.Y., Liu, Z.C., Liu, X.C. and Ji, W.Q. (2015) Himalayan leucogranite: Petrogenesis and implications to orogenesis and plateau uplift. Acta Petrologica Sinica, 31, 1–36 (in Chinese with English abstract).

Wu, F.Y., Liu, X.C., Liu, Z.C., Wang, R.C., Xie, L., Wang, J.M., Ji, W.Q., Yang, L., Liu, C., Khanal, G.P., and He, S.X. (2020) Highly fractionated Himalayan leucogranites and associated rare-metal mineralization. Lithos, 352–353. doi: 10.1016/j.lithos.2019.105319.

Xie, L., Tao, X., Wang, R., Wu, F., Liu, C., Liu, X., Li, X., and Zhang, R. (2020) Highly fractionated leucogranites in the eastern Himalayan Cuonadong dome and related magmatic Be–Nb–Ta and hydrothermal Be–W–Sn mineralization. Lithos, 354–355. doi: 10.1016/j.lithos.2019.105286.

Yang, S.Y., Jiang, S.Y., and Palmer, M.R. (2015) Chemical and boron isotopic compositions of tourmaline from the Nyalam leucogranites, South Tibetan Himalaya: Implication for their formation from B-rich melt to hydrothermal fluids. Chemical Geology, 419, 102–113.

Yin, A. (2006) Cenozoic tectonic evolution of the Himalayan orogen as constrained by along-strike variation of structural geometry, exhumation history, and foreland sedimentation. Earth-Science Reviews, 76, 1–131.

Yin, A., and Harrison, T.M. (2000) Geologic evolution of the Himalayan-Tibetan orogen. Annual Review of Earth and Planetary Sciences, 28, 211–280.

Zeng, L.S., Gao, L.E., Xie, K.J., and Liu-Zeng, J. (2011) Mid-Eocene high Sr/Y granites in the Northern Himalayan Gneiss Domes: Melting thickened lower continental crust. Earth and Planetary Science Letters, 303, 251–266.

Zhou, Q., Li, W., Wang, G., Liu, Z., Lai, Y., Huang, J., Yan, G., and Zhang, Q. (2019) Chemical and boron isotopic composition of tourmaline from the Cuonadong leucogranite-pegmatite system in South Tibet. Lithos, 326-327, 529–539.

Manuscript received May 15, 2020
Manuscript accepted June 4, 2020
Manuscript handled by Calvin Barnes

Endnote:

[1]Deposit item AM-20-97608, Supplemental Material. Deposit items are free to all readers and found on the MSA website, via the specific issue's Table of Contents (go to http://www.minsocam.org/MSA/AmMin/TOC/2020/Sep2020_data/Sep2020_data.html).